Extreme Mechanics Letters 37 (2020) 100727

Contents lists available at ScienceDirect

Extreme Mechanics Letters

journal homepage: www.elsevier.com/locate/eml

On the solid-state-bonding mechanism in friction stir welding

Xue Wang [a], Yanfei Gao [a,*], Martin McDonnell [b], Zhili Feng [c,*]

[a] Department of Materials Science and Engineering, University of Tennessee, Knoxville, TN 37996, USA
[b] US Army Tank Automotive Research Development and Engineering Center, Warren, MI 48397, USA
[c] Materials Science and Technology Division, Oak Ridge National Laboratory, Oak Ridge, TN 37831, USA

ARTICLE INFO

Article history:
Received 23 January 2020
Received in revised form 3 April 2020
Accepted 3 April 2020
Available online 10 April 2020

Keywords:
Friction stir welding
High temperature bonding
Creep-controlled cavity closure

ABSTRACT

A critical assessment of various solid-state-bonding mechanisms is established for friction stir welding (FSW) processes of engineering alloys. The commonly assumed sintering-like diffusional-bonding hypothesis is criticized in this work as not the dominant mechanism. For the wide spectrum of material constitutive laws and FSW processing conditions examined and employed in realistic applications, the thermomechanical history on the workpiece–workpiece interface traverses in the creep-dominated regime for the growth/shrinkage of interfacial cavities. The evolution of the bonding fraction relies mainly on the creep strain rate in the adjourning workpieces, weakly on stress triaxiality, and negligibly on interfacial diffusion.

1. Introduction

Friction stir welding (FSW) is a quintessential solid-state-bonding technology, in which the workpieces are metallurgically bonded at the interface, under significant heating from tool–workpiece frictional sliding and plastic deformation in the workpieces [1,2]. In contrast to the solidification processes involved in conventional welding techniques, no bulk melting is involved in friction stir welded joints. An inherent advantage of FSW is thus its immunity from defects and property deteriorations associated with solidification, as solidification cracking, porosity, and melting and coarsening of strengthening phases are eliminated in this technique. In addition, the extensive thermomechanical deformation of FSW refines the microstructure of the weld region, and may lead to significant enhancement of weld mechanical properties such as tensile strength and toughness [3]. Hence, whereas fusion welding generally results in weld property degradation, FSW can produce a weld with mechanical properties similar to or even better than those of the base metal. This is particularly a very important aspect of FSW, as the weld region made by the fusion welding processes are often the weakest region for a variety of high-performance engineering materials. From the viewpoint of materials processing, it has been found that strain rate, temperature, and stress fields are affected both by thermomechanical processing parameters in FSW such as the tool geometry, traveling speed, and rotation speed and by the properties of the joining materials. A multitude of experimental and numerical studies, including computational fluid dynamics (CFD) and finite element method (FEM), have been conducted to understand the characteristics of the thermomechanical fields [4–6]. A mechanistic understanding of the dependence of bonding evolution on processing parameters and materials behavior is of critical importance, which will eventually affect the structural integrity of the weldments. Studies along this line, however, remains elusive as explained below.

Even though both FSW and conventional diffusion bonding technologies are solid-state bonding in nature, it takes much shorter time in FSW to form the bonding at the interface. In conventional solid-state diffusion bonding processes, it is often understood that the interface free energy reduction as in the sintering process and the applied joining pressure drive the closure of gaps (e.g., from isolated adjourning domains, to meandering tunnels, and to discrete cavities with the increase of the degree of bonding), while the kinetics is governed by the interfacial mass transport at elevated temperatures [7,8]. Thus it is found that pressure, temperature and bonding time are key factors that could affect the bonding fraction. On the other hand, time elapses rapidly in FSW processes so that the contribution of diffusional processes might be limited (as will be proved so in this paper). Previous experimental studies conclude empirically that the degree of bonding tends to increase when the applied force/torque and the resulting temperature field are high, but does not change much with respect to the increase of the abutting force (i.e., the lateral force that holds the two workpieces together), which suggest the critical role of creep rather than diffusion on the bonding evolution. In the criterion developed in [9], a parameter that controls the final solid-state bonding was defined to depend on the pressure and the effective stress on the interface. A sound bonding is believed to be attached when this

* Corresponding authors.
E-mail addresses: ygao7@utk.edu (Y. Gao), fengz@ornl.gov (Z. Feng).

https://doi.org/10.1016/j.eml.2020.100727
2352-4316/

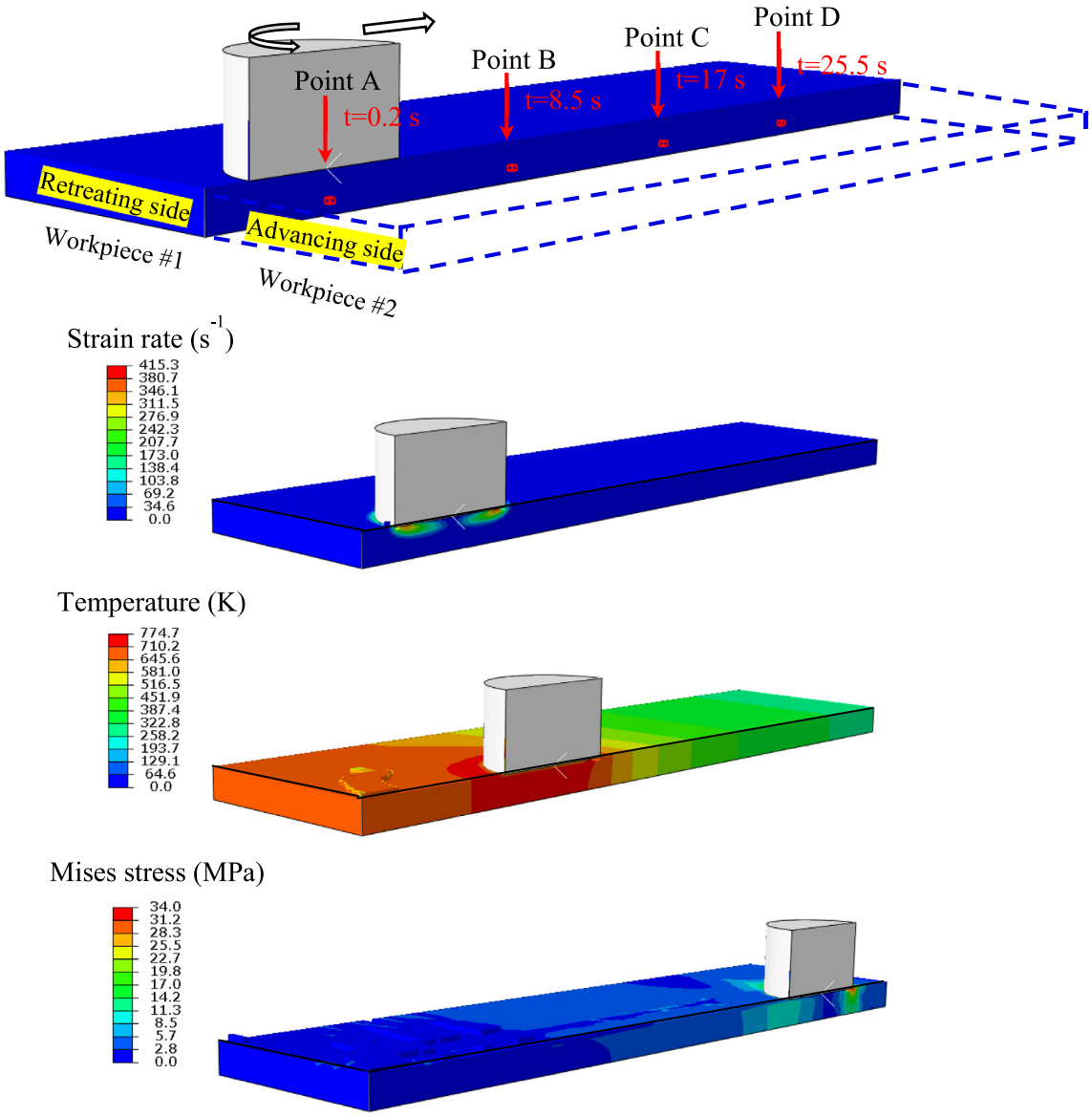

Fig. 1. Finite element setup using the coupled Eulerian–Lagrangian (CEL) approach in the friction stir welding (FSW) process. Representative results of the strain rate, temperature, and Mises stress fields are given with their corresponding tool locations, where the graininess on the workpiece surface results from plastic flow.

parameter reaches a critical value. However, no clear mechanisms that control the bonding evolution are clarified in regards to the evolution of this parameter. Chen et al. [10] suggested that the interfacial bonding depends on the viscoplastic crushing of the surface asperities of the two workpieces. Such a model shines key insights on the bonding evolution, but it requires a knowledge of surface roughness, its applicable parametric space has not been given, and the stress triaxiality (i.e., the relative contribution of pressure and shear) is not included.

The unique view in this work is motivated by the deformation and failure mechanism maps in polycrystalline materials [11, 12]. Grain boundary diffusional processes are only important at low stress and high temperature, in contrast to the dislocation creep at high stress. The closure of the workpiece–workpiece gap field is a reverse process of intergranular fracture due to cavity growth; the latter may be determined by the interfacial diffusion in the classic Hull–Rimmer model [13], or by the creep-driven growth, or by their competition as governed by the Needleman–Rice length scale [14]. Consequently, a quantitative understanding of the solid-state bonding in FSW relies on a quantitative assessment of the temporal evolution of the stress, strain rate, and temperature fields on the workpiece–workpiece interface, and thus the rigorous determination of the competing roles of interfacial diffusion and creep in the surrounding workpieces. In this work, we will first report our simulated transient temperature, stress, and strain rate fields in FSW by using the Coupled Eulerian–Lagrangian (CEL) finite element method in the commercial software, ABAQUS [15]. The thermomechanical histories of four representative reference points on the interface are compared to both the deformation mechanism map and the contour plots of the Needleman–Rice length, which upholds that creep-dominated cavity closure be the solid-state bonding mechanism. A quantitative prediction of the bonding fraction will be presented for these four reference points, and implications on FSW processing parameters and materials parameters will be discussed.

2. Friction stir welding simulation

As shown in Fig. 1, the finite element setup using the CEL method includes the sample domain (only the workpiece on the

retreating side of the tool is shown here) and the "empty" domain (not shown for clarity; for heat transfer analysis only). It should be noted that the commonly used CFD simulations for FSW face difficulties in modeling the tool–workpiece frictional behavior since pressure has to be specified *a priori* (such as through the user-defined function in a commercial CFD software, FLUENT). How and what kind of interface boundary condition is applied will significantly change the final simulation results. FEM simulations avoid this problem by directly simulating the Coulomb friction, but the severe plastic deformation cannot be handled in the standard Lagrangian approach, which can be resolved by the CEL approach. The CEL approach divides the entire control volume into Eulerian and Lagrangian domains, thus overcoming the difficulty in frictional modeling in CFD and the difficulty in large deformation in computational solid mechanics. In Fig. 1, since our objective is devoted to the bonding analysis, for the sake of simplicity, the rotating tool is modeled without pin. The entire FSW process includes plunging, dwelling, and welding, for which the spin rate and welding speed are 1000 rpm and 2 mm/s, respectively. We choose four reference points (A–D in Fig. 1) on the workpiece–workpiece interface, with the corresponding times when the tool reaches them correspondingly. A steady state obviously is reached upon arriving at Point C.

Considering the extremely high stress and temperature, the power-law creep breaks down, and the hyperbolic sine law is used [11],

$$\dot{\varepsilon}_{creep} = A_n \left[\sinh\left(\frac{\sigma_e}{\sigma_{ref}}\right)\right]^n \exp\left(-\frac{Q}{RT}\right), \tag{1}$$

where σ_e is the effective Mises stress, σ_{ref} is the reference stress, A_n is a pre-factor, n is the stress exponent, Q is the activation energy for dislocation creep, R is the gas constant, and T is the absolute temperature. The material of interest is precipitate-strengthened aluminum alloy, Al6061-T6, and the corresponding material parameters include: $A_n = 2.41 \times 10^7 s^{-1}$, $n = 3.55$, $\sigma_{ref} = 22.22$ MPa, $Q = 145$ kJ/mol, and $T_m = 856$ K [16,17].

Representative results given in Fig. 1 are for strain rate, temperature, and Mises stress fields when the tool arrives Points A, B, and D, respectively. The temperature field extends to a much wider regime than the strain rate and stress fields. The thermo-mechanical histories of these four traced positions are given in the deformation mechanism map in Fig. 2(a). The background contours are for the strain rate by the dislocation creep law in Eq. (1). The trajectories for all four points, except the early stage of that of Point A, almost collapse onto one another. The stress rises up to high flow strength at low temperature, and then heating from both tool–workpiece friction and plastic deformation leads to the increase of temperature and the corresponding stress decrease due to thermal softening. Even after the tool passes these reference points, the temperature still remains high (as can be seen from the third row in Fig. 1), but the stress drops rapidly due to the departure of the spinning tool. The boundaries between dislocation creep in Eq. (1) and Coble creep that arises from grain boundary diffusion are also shown in Fig. 1(a) for grain sizes of 10 and 100 μm. Can we now conclude that diffusional processes do not contribute noticeably to the bonding process? This answer is no, since the interfacial cavity closure is governed by the competition by interfacial diffusion and creep in the surrounding materials, which can only be determined from the Needleman–Rice length scale in Fig. 2(b).

We should also point out that these trajectories are universal for other materials as well, because the thermal softening will eventually slow down the heat generation rate by plastic flow, and thus these trajectories plummet at the final stage.

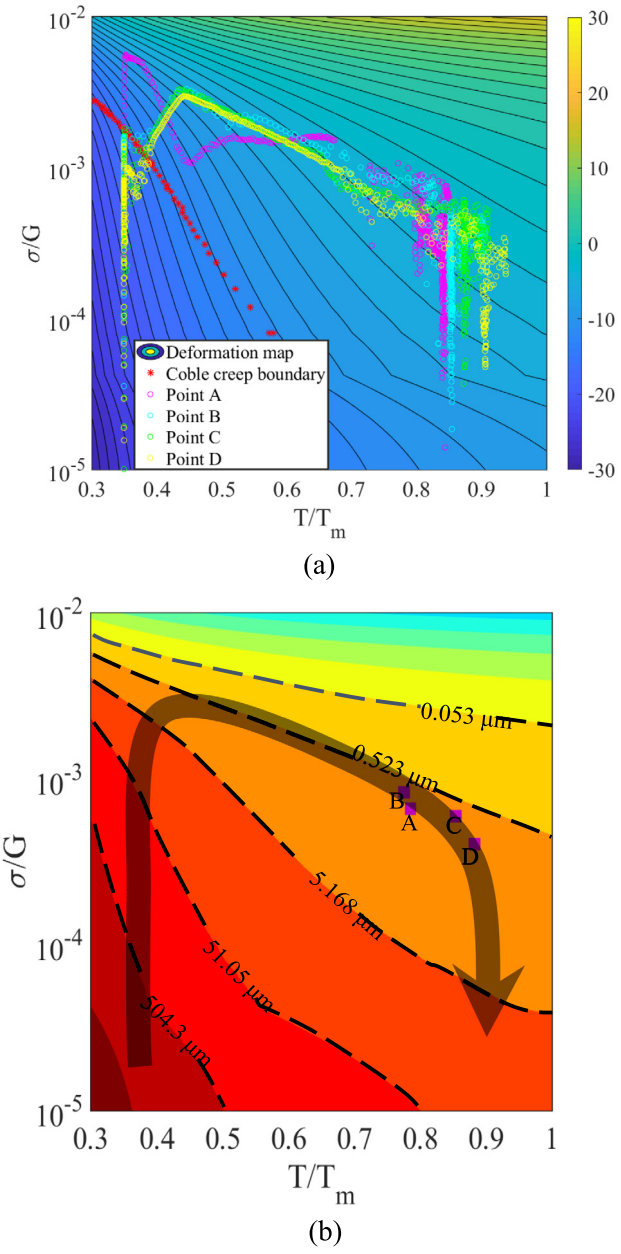

Fig. 2. (a) Thermomechanical histories of the four reference points are plotted on top of the deformation mechanism map of Al6061-T6 alloy. These histories are located in the dislocation creep regime. (b) Contour plot of the Needleman–Rice length scale, L_{NR}, with respect to the normalized stress and the homologous temperature. The thermomechanical histories are schematically overlaid on this plot. The discrete squares indicate the occurrence of full bonding for the four reference points.

3. Cavity closure as the bonding process

A unit process during the interfacial bonding is the shrinkage of the interfacial cavities in Fig. 3, which is the reverse process of the cavity growth in high temperature fracture. These cavities are lens-like because of the surface tension balance at the high temperature. The bonding fraction is given by $f_b = 1 - f_h$, where $f_h = (a/b)^2$ is the area fraction of these cavities/holes, and a and b are cavity size and cavity spacing, respectively. Based on a modification by Cocks and Ashby [18] to the classic Hull–Rimmer model, the evolution of interfacial cavity is

$$\frac{df_b}{dt} = -\frac{2(1-f_b)}{a^3 \ln[1/(1-f_b)]} \cdot \frac{D_B \delta_B \Omega}{k_B T} \cdot \sigma_n = -\frac{2(1-f_b)}{\ln[1/(1-f_b)]}$$

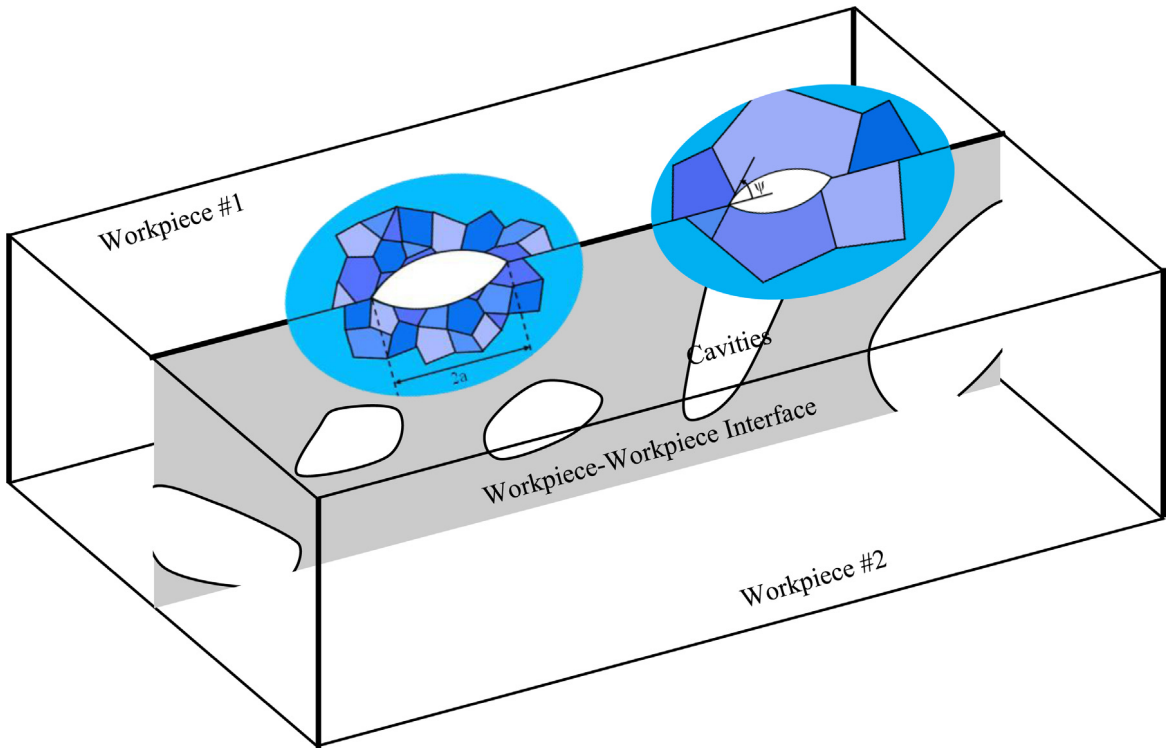

Fig. 3. Schematic illustrations of bonded and unbonded regimes on the workpiece–workpiece interface. Cavities tend to be lens like because of the balance of surface tensions, but they may coalescence into meandering stripes at a low degree of bonding.

$$\times\ \dot{\varepsilon}^{eff}_{creep}\left(\frac{\sigma_n}{\sigma_e}\right)\left(\frac{L_{NR}}{a}\right)^3, \tag{2}$$

where D_B is the interfacial diffusion coefficient, δ_B is the interface boundary thickness (usually several atomic sizes), Ω is atomic volume, and k_B is the Boltzmann's constant. The combination of diffusivity and k_BT arises from the Nernst–Einstein relationship. When the applied normal stress is tensile/compressive, the bonding fraction decreases/increases accordingly. The conversion to the use of the effective creep rate, $\dot{\varepsilon}^{eff}_{creep}$, and the Needleman–Rice length, L_{NR}, will be discussed shortly.

The cavity can growth or shrink when there is a creep deformation in the surrounding material. Under the multiaxial stress state, extensive numerical simulation results by Sham and Needleman [19] can be fitted to

$$\frac{1}{f_b}\cdot\frac{df_b}{dt} = -(1-f_b)\,\dot{\varepsilon}^{eff}_{creep} \times \begin{cases} \left[\alpha_n\left|\dfrac{\sigma_m}{\sigma_e}\right|+\beta_n\right]^n \operatorname{sgn}\left(\dfrac{\sigma_m}{\sigma_e}\right), & if\ \left|\dfrac{\sigma_m}{\sigma_e}\right| > 1 \\ [\alpha_n+\beta_n]^n\,\dfrac{\sigma_m}{\sigma_e}, & if\ \left|\dfrac{\sigma_m}{\sigma_e}\right| \le 1 \end{cases} \tag{3}$$

where dimensional parameters are $\alpha_n = 3n/2$ and $\beta_n = (n-1)(n+0.4319)/n^2$, sgn () is the sign function, and σ_m is the mean stress. We have added a multiplicative factor of $1/f_b$ to the left hand side of Eq. (3), without which the original Sham–Needleman equation only works when f_b is larger than a critical value (e.g., 0.4). The comparison between the diffusional and creep processes in Eqs. (2) and (3) defines the Needleman–Rice length scale,

$$L_{NR} = \left[\frac{D_B\delta_B\Omega}{k_BT}\cdot\frac{\sigma_e}{\dot{\varepsilon}^{e}_{creep}}\right]^{1/3}. \tag{4}$$

This can also be viewed as a kinematic constraint, that is, if the interfacial diffusion is not divergence free, the surrounding materials must creep to ensure continuity.

Contours of L_{NR} are given in Fig. 2(b) for our aluminum alloy. When L_{NR} is larger than cavity size, the cavity closure is governed by interfacial diffusion. A small L_{NR} corresponds to the creep dominant closure of cavities, as shown by the term of $(L_{NR}/a)^3$ in Eq. (2). The stress–temperature trajectories in Fig. 2(a), if plotted on top of Fig. 2(b), will indicate that our reference point will only enter the large-L_{NR} regime when the tool passes it (i.e., temperature still remaining high but stress decreasing dramatically).

Thermomechanical history data for these four reference points are used as inputs to Eq. (3), which is then integrated implicitly to predict the evolution of f_b. Two initial values are chosen, with $f_b|_{t=0} = 0.8$ representing finely polished workpieces and 0.01 for rough surfaces. Such a choice helps avoid the need to conduct experimental characterization of interface morphology. As shown in Fig. 4, along with the movement of the tool, the area fraction of cavities, f_h, remains almost unchanged until the reference point falls into the thermomechanical process zone. Referring back to Fig. 1, one can see that although the temperature field extends to a much larger zone, the strain rate field is rather narrowly localized near the tool. The evolution of f_b is directly governed by $\dot{\varepsilon}^{eff}_{creep}$, but not by T. Before the tool moves right to the top of the reference point, f_b rapidly increases to unity even with a very small $f_b|_{t=0}$, indicating that a full degree of bonding can be achieved mainly by creep before the reference point falls into the wake of the tool. An additional calculation is presented by the dashed line in which Eq. (2) is added onto the evolution of f_b. Before a full bonding is reached, both the temperature and stress at this reference point D are high, corresponding to the regime in Fig. 2(b) with L_{NR} being around several microns. Even with the choice of $a = 1$ μm, the diffusion-driven reduction of f_b has little contribution to the overall evolution.

The generality of our model can also be confirmed from the discrete squares in Fig. 2(b), which indicate the occurrence of full bonding for these four reference points. The Needleman–Rice contour plots are quite universal with respect to the normalized

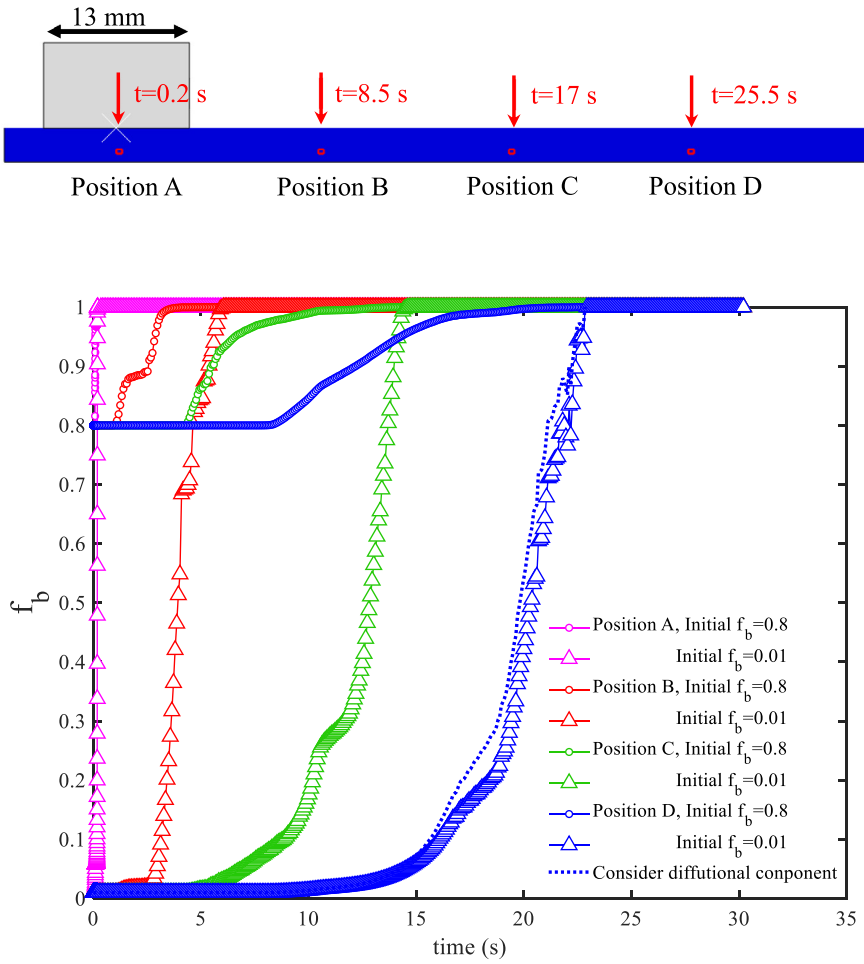

Fig. 4. The evolution of f_b (i.e., the area fraction of bonding and no cavities) for the four reference points, with two initial values representing smooth and rough workpiece–workpiece interface. All these curves rapidly drop to zero, indicating that the full bonding is roughly accomplished when the tool arrives roughly above the reference point. The addition of diffusional contribution, as shown by the dashed line, has little effect on this solid-state-bonding process.

stress and temperature, as this length in Eq. (4) is primarily dictated by the stress exponent and the difference between the creep activation energy in Eq. (1) and the diffusion activation energy of D_B in Eq. (2). During the friction stir welding, the temperature rise softens the material and thus decreases the heat generation rate by plastic flow, and then the temperature rise slows down, which naturally leads to the universal trajectory in Fig. 2(b). Full bonding occurs at locations with very low Needleman–Rice length values, so that diffusional bonding plays a secondary role as compared to creep-induced cavity closure.

4. Conclusion

In summary, from the simulated thermomechanical histories of a number of reference points on the workpiece–workpiece interface, we find out the interface traverses in regimes with very low L_{NR}, thus indicating the dominance of creep-controlled cavity closure. The evolution rate of the interfacial bonding depends primarily on the creep strain rate in the surrounding workpieces abutting at the interface, but not on the far-reaching temperature field. This study helps reveal design strategies in promoting the solid-state bonding in FSW by entering and staying in the creep-dominant interfacial cavity closure through tuning materials constitutive parameters, thermomechanical processing parameters, and geometric shape factors.

Declaration of competing interest

The authors declare that they have no known competing financial interests or personal relationships that could have appeared to influence the work reported in this paper.

Acknowledgments

The authors would like to acknowledge the Manufacturing and Materials Joining Innovation Center (Ma^2JIC), made possible through IIP-1540000 and IIP-1822186 from the US National Science Foundation, Industry University Cooperative Research Center (I/UCRC) program, to the University of Tennessee for financial support. XW and YG are grateful to fruitful discussions with Dr. Wei Zhang at ORNL, and to the partial support from the Center for Materials Processing at the University of Tennessee.

References

[1] R.S. Mishra, Z.Y. Ma, Mater. Sci. Eng. R. 50 (2005) 1–78.
[2] R. Nandan, T. DebRoy, H.K.D.H. Bhadeshia, Prog. Mater. Sci. 53 (2008) 980–1023.
[3] Z. Feng, R.J. Steel, S.M. Packer, S.A. David, Proceedings of the ASME Pressure Vessels and Piping Conference, Vol. 6, 2009, pp. 776–779.
[4] K.L. Nielsen, T. Pardoen, V. Tvergaard, B. de Meester, A. Simar, Int. J. Solids Struct. 47 (2010) 2359–2370.
[5] X. Liu, G. Chen, J. Ni, Z. Feng, J. Manuf. Sci. Eng. 139 (2017) 051004.
[6] M. Reza-E-Rabby, K. Ross, N.R. Overman, M.J. Olszta, M. McDonnell, S.A. Whalen, Scr. Mater. 148 (2018) 63–67.

[7] J. Pilling, Mater. Sci. Eng. 100 (1988) 137–144.
[8] B. Derby, E. Wallach, Met. Sci. 16 (1982) 49–56.
[9] M. Plata, J. Piwnik, Proceedings of International Aluminum Extrusion Technology Seminar, Vol. 1, 2000, pp. 205-212.
[10] G. Chen, et al., Scr. Mater. 128 (2017) 41–44.
[11] M. Ashby, Adv. Appl. Mech. 23 (1983) 117–177.
[12] W. Zhang, X. Wang, Y. Wang, X. Yu, Y. Gao, Z. Feng, J. Mech. Phys. Solids 134 (2020) 103775.
[13] D. Hull, D.E. Rimmer, Phil. Mag. 4 (1959) 673–687.
[14] A. Needleman, J.R. Rice, Acta Metall. 28 (1980) 1315–1332.
[15] ABAQUS 6.14 User's Manual, Dassault Systèmes, 2014.
[16] T. Sheppard, A. Jackson, Mater. Sci. Technol. 13 (1997) 203–209.
[17] R. Crawford, G. Cook, A. Strauss, D. Hartman, M. Stremler, Sci. Technol. Weld. Join. 11 (2006) 657–665.
[18] A. Cocks, M. Ashby, Prog. Mater. Sci. 27 (1982) 189–244.
[19] T.L. Sham, A. Needleman, Acta Metall. 31 (1983) 919–926.